Hindawi
Geofluids
Volume 2018, Article ID 6385252, 14 pages
https://doi.org/10.1155/2018/6385252

WILEY | Hindawi

Research Article

Diagnosis of Water-Influx Locations of Horizontal Well Subject to Bottom-Water Drive through Well-Testing Analysis

Jiazheng Qin, Shiqing Cheng, Youwei He, Dingyi Li, Le Luo, Xinzhe Shen, and Haiyang Yu

State Key Laboratory of Petroleum Resources and Prospecting, China University of Petroleum, Beijing 102249, China

Correspondence should be addressed to Shiqing Cheng; chengsq@cup.edu.cn

Received 16 October 2017; Revised 4 January 2018; Accepted 10 September 2018; Published 25 November 2018

Guest Editor: Zhien Zhang

Horizontal well (HW) has been widely applied to enhance well productivity and prevent water coning in the anisotropic reservoir subject to bottom-water drive. However, the water-cut increases quickly after only one or two years' production in China while oil recovery still keeps at a very low level. It becomes a major challenge to effectively estimate production distribution and diagnose water-influx locations. Ignoring the effect of nonuniform production distribution along wellbore on pressure response may cause erroneous results especially for water-influx location determination. This paper developed an analytical method to determine nonuniform production distribution and estimate water-influx sections through well-testing analysis. Each HW is divided into multiple producing segments (PS) with variable parameters (e.g., location, production, length, and skin factor) in this model. By using Green's functions and the Newman-product method, the novel transient pressure solutions of an HW can be obtained in the anisotropic reservoir with bottom-water drive. Secondly, the influences of nonuniform production-distribution on type curves are investigated by comparing the multisegment model (MSM) with the whole-segment model (WSM). Results indicate that the method proposed in this paper enables petroleum operators to interpret parameters of reservoir and HW more accurately by using well-testing interpretation on the basis of bottom-hole pressure data and further estimate water-influx sections and nonproducing segments. Additionally, relevant measures can be conducted to enhance oil production, such as water controlling for water-breakthrough segments and stimulation treatments for nonproducing locations.

1. Introduction

Horizontal well technology is well established for enhancing well productivity of low-permeability reservoirs, especially for reservoirs with bottom water or gas cap [1–8] and unconventional oil and gas resources [9]. However, oil production decreases sharply when the water front arrives at the horizontal wellbore so that well performance is much worse than expected [10, 11]. How to effectively evaluate the well performance and reservoir performance becomes significant [12–14], including estimating production distribution and diagnosing water-influx segments [15, 16]. On the one hand, production logging has been carried out to obtain fluid-flow profiles and determine water breakthrough sections for many years [17]. Two examples were presented by Al-Behair et al. [18] to diagnose gas entry intervals by advanced production logging. Al-Muthana et al. [19] elaborated flow profiles by using an integrated compact production logging tool. Later, Bawazir et al. [10] presented three field examples on data logging in dead horizontal wells and interpretation to pinpoint water-influx intervals. Aibazarov et al. [20] described how to determine the downhole fluid flow path and further to optimize water shut-off operations by using integrating data from spectral noise logging tools and multisensor production logging. Over the past few years, many researchers pinpointed water entry intervals through production logging [21–36]. On the other hand, another monitoring system can provide vital data (e.g., pressure and temperature) for water-influx detection. Marquardt [27] developed the Levenberg-Marquardt algorithm for inverting temperature and pressure data into desired inflow rates. Later, several interpretation studies were conducted on how to obtain production profiles by matching measurable data (e.g., pressure, temperature, and density) [28–30]. Bui et al. [31] diagnosed inflow

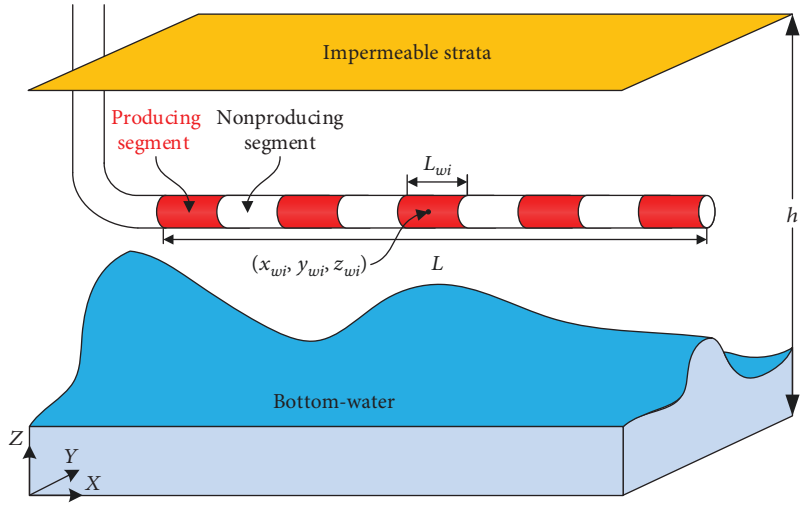

Figure 1: Physical model of MSHW subject to bottom water drive.

behavior in horizontal wells and identified intervals of fluid influx by examining wellbore pressure sensing at multiple points. Based on the variation of the pressure gradient in the wellbore, water influx location can be identified based on trending analysis according to data delivered by sensors [32]. Yoshioka et al. [33–35] presented synthetic and field examples for interpreting the flow profile of single phase by using the inversion model. Li and Zhu [36] improved this model and developed a transient, 3D, multiphase reservoir model to predict pressure and temperature distribution. However, important data (e.g., pressure, temperature, and flow rate) at multiple points along the wellbore cannot be obtained since this monitoring system such as the production logging test is difficult to implement in some situations. Thus, well testing becomes a preferred choice.

Pressure transient analysis (PTA) has been extensively used for evaluating production performance of horizontal wells [5, 37–45]. Kamal et al. [44] pointed out that even if the horizontal well is entirely open or perforated, some of the segments are nonproducing. He et al. [45] and Qin et al. [46] established a PTA model to estimate the effective producing length and identify locations of underperforming horizontal segments. Detailed description about PTA of MSM can be found in He et al. [45]. Additionally, this phenomenon of nonuniform production distribution also exists in multifractured horizontal wells [47–52]. Some works pointed out that the phenomenon is mainly caused by reservoir heterogeneity, formation damage, and selective completion [52, 53].

However, these models are not applicable for an HW in the reservoir subject to bottom-water drive. To fill this gap, this paper develops a novel approach to detect water entry of a horizontal well in a low-permeability bottom-water drive reservoir considering nonuniform production rate distribution through PTA.

2. Model

2.1. Physical Model. The physical model is shown in Figure 1. Some assumptions are needed to derive the practical solutions of this transient-flow model.

(1) There is an MSHW located in the horizontal-slab reservoir with an upper impermeable stratum and a lower bottom-water boundary. The formation is infinite in the horizontal direction. The horizontal-slab reservoir is considered to be anisotropic and homogeneous, and it has a constant thickness (h), permeability ($k_h = k_x = k_y$ and $k_v = k_z$ in horizontal and vertical directions), porosity (ϕ), initial reservoir pressure (p_i), and total compressibility (C_t).

(2) The HW is parallel to the x-axis and divided into multiple segments. The length, production rate, and skin factor of the i^{th} segment can be defined as L_{wi}, q_{wi}, and S_{wi}, and the total length of HW is equal to L. The point (x_{wi}, y_{wi}, and z_{wi}) is the center of the i^{th} segment.

(3) The fluid is single-phase, and the total production rate is q.

(4) The effects of capillary and gravity are ignored.

2.2. Mathematical Model. The transient-flow equation can be written as

$$\begin{aligned} \frac{\partial^2 p}{\partial x^2} + \frac{\partial^2 p}{\partial y^2} + \frac{\partial^2 p}{\partial z^{*2}} &= \frac{1}{\eta}\frac{\partial p}{\partial t}, \\ z^* &= z\sqrt{\frac{k_h}{k_v}} = \frac{z}{\beta}, \\ \eta_h &= \frac{k_h}{\phi\mu C_t}, \\ \eta_v &= \frac{k_v}{k_h}\eta_h = \beta^2\eta_h, \end{aligned} \tag{1}$$

where z^* is defined to characterize the permeability heterogeneity. η_h and η_v represent the diffusivities in horizontal and vertical directions, respectively.

In the horizontal-slab reservoir, the individual horizontal segment can be considered as a line source with length L_{wi}. By use of the instantaneous-source solutions [54, 55] and the Newman-product principle [56], the pressure drop caused by the i^{th} segment can be expressed as

$$\Delta p(x,y,z,t) = p_{\text{i}} - p(x,y,z,t) = \frac{1}{\phi C_{\text{t}}} \frac{q_{wi}}{L_{wi}} \int_0^t G_x G_{yz} d\tau, \quad (2)$$

where

$$\begin{aligned} G_x &= \frac{1}{2}\left\{ \text{erf}\left[\frac{L_{wi}/2 + (x - x_{wi})}{\sqrt{4\eta_{\text{h}}\tau}}\right] + \text{erf}\left[\frac{L_{wi}/2 - (x - x_{wi})}{\sqrt{4\eta_{\text{h}}\tau}}\right]\right\}, \\ G_{yz} &= \frac{1}{\sqrt{4\pi\eta_{\text{h}}\tau}} \exp\left[-\frac{(y - y_{wi})^2}{4\eta_{\text{h}}\tau}\right] \\ &\quad \cdot \frac{2}{h^*} \sum_{n=1}^{\infty} \left\{ \exp\left[-\frac{(2n-1)^2\pi^2\eta_{\text{v}}\tau}{4h^{*2}}\right] \cos\left[\frac{(2n-1)\pi z_{wi}}{2h}\right] \right. \\ &\quad \left. \cdot \cos\left[\frac{(2n-1)\pi z}{2h}\right]\right\}, \\ h^* &= h\sqrt{\frac{k_{\text{h}}}{k_{\text{v}}}} = \frac{h}{\beta}, \end{aligned} \quad (3)$$

where τ is the time variable and h^* means the reservoir thickness considering the effect of anisotropy.

Dimensionless variables are defined by

$$\begin{aligned} p_{\text{D}} &= \frac{2\pi k_{\text{h}} h^* [p_{\text{i}} - p(x,y,z,t)]}{q\mu}, \\ t_{\text{D}} &= \frac{k_{\text{h}} t}{\phi\mu C_{\text{t}} L^2} = \eta_{\text{h}} \frac{t}{L^2}, \\ h_{\text{D}}^* &= \frac{h^*}{L}, \\ r_{w\text{D}} &= \frac{r_w}{L}, \\ x_{\text{D}} &= \frac{x}{L}, \\ y_{\text{D}} &= \frac{y}{L}, \\ z_{\text{D}} &= \frac{z}{L}, \\ x_{wi\text{D}} &= \frac{x_{wi}}{L}, \\ y_{wi\text{D}} &= \frac{y_{wi}}{L}, \\ z_{wi\text{D}} &= \frac{z_{wi}}{L}, \\ L_{wi\text{D}} &= \frac{L_{wi}}{L}, \\ L_{Di} &= \frac{L_{wi}}{h^*}, \\ C_{\text{D}} &= \frac{C}{2\pi h^* \phi C_{\text{t}} L^2}, \\ q_{wi\text{D}} &= \frac{q_{wi}}{\sum_{i=1}^{N} q_{wi}}. \end{aligned} \quad (4)$$

The analytical solution of pressure drop of an MSHW subject to bottom water drive can be expressed as

$$p_{\text{D}}(x_{\text{D}}, y_{\text{D}}, z_{\text{D}}, t_{\text{D}}) = \sum_{i=1}^{N} \sqrt{\pi} \frac{q_{wi\text{D}}}{L_{wi\text{D}}} \int_0^{t_{\text{D}}} G_{x\text{D}} G_{yz\text{D}} d\tau_{\text{D}}, \quad (5)$$

where

$$\begin{aligned} G_{x\text{D}} &= \text{erf}\left[\frac{L_{wi\text{D}}/2 + (x_{\text{D}} - x_{wi\text{D}})}{\sqrt{4t_{\text{D}}}}\right] + \text{erf}\left[\frac{L_{wi\text{D}}/2 - (x_{\text{D}} - x_{wi\text{D}})}{\sqrt{4t_{\text{D}}}}\right], \\ G_{yz\text{D}} &= \frac{1}{\sqrt{t_{\text{D}}}} \exp\left[-\frac{\left(y_{\text{D}} - y_{yz\text{D}}\right)^2}{4t_{\text{D}}}\right] \\ &\quad \cdot \sum_{n=1}^{\infty} \left\{ \exp\left[-\frac{(2n-1)^2\pi^2\beta^2 t_{\text{D}}}{4h_{\text{D}}^{*2}}\right] \cos\left[\frac{(2n-1)\pi z_{\text{D}}}{2h_{\text{D}}}\right] \right. \\ &\quad \left. \cdot \cos\left[\frac{(2n-1)\pi z_{wi\text{D}}}{2h_{\text{D}}}\right]\right\}. \end{aligned} \quad (6)$$

There exists formation damage around the HW during the process of drilling, completion, production, and other operations [52]. The skin factor (S) was introduced by Van Everdingen [57] to quantitatively characterize the effect of formation damage on transient-pressure behaviors. The dimensionless transient-pressure solution considering the effect of skin factor is

$$p_{\text{SD}}(x_{\text{D}}, y_{\text{D}}, z_{\text{D}}, t_{\text{D}}) = \sum_{i=1}^{N} \left(\sqrt{\pi} \int_0^{t_{\text{D}}} \frac{q_{wi\text{D}}}{L_{wi\text{D}}} G_{x\text{D}} G_{yz\text{D}} d\tau_{\text{D}} + \frac{q_{wi\text{D}}}{L_{\text{D}i}} S_{wi} \right), \quad (7)$$

where S_{wi} means the skin factor of an individual segment. Van Everdingen and Hurst [58] proposed that the wellbore-storage effect can be incorporated by converting the solutions into the Laplace space. The dimensionless transient-pressure solution considering the wellbore-storage effect can be expressed as

$$p_w D(C_{\text{D}}, u) = \int_0^{t_{\text{D}}} \left[1 - C_{\text{D}} \frac{dp_{w\text{D}}}{dt_{\text{D}}}\right] \frac{dp_{\text{SD}}(t-\tau)}{d\tau} d\tau, \quad (8)$$

where u is the Laplace variable. Therefore, the transient-pressure solution in the Laplace space of an MSHW

subject to bottom-water drive can be obtained by considering the skin-factor and wellbore-storage effect by use of Laplace transformation.

$$\bar{p}_{wD}(C_D, S, u) = \frac{\bar{p}_{SD}(u)}{1 + u^2 C_D \bar{p}_{SD}(u)}, \tag{9}$$

where $\bar{p}_{wD}$ is the dimensionless pressure solution in the Laplace space. Finally, the pressure solution in real space can be obtained through a numerical algorithm [59].

3. Pressure-Transient Analysis

First, type curves are developed and flow regimes of MSHW subject to bottom water drive are discussed. Further, we analyze the effects of main parameters on pressure transient behavior (PTB).

3.1. Flow Regimes of WSM. The pressure response of WSM for different lengths of HW is shown in Figure 2. Compared with the models in the reservoir without bottom-water drive, early flow regimes still can be recognized easily (i.e., wellbore-storage flow, transitional flow, and steady flow regime), while the late pressure behaviors may be covered due to the effect of bottom water. Radial flow occurs between transitional flow and steady flow regimes when the HW is long enough (e.g., $L_D = 0.9$, 1.5, 2.1, 2.7). Furthermore, the duration of radial flow becomes shorter as L_D decreases. Finally, the radial flow would be covered when L_D is short enough (e.g., $L_D = 0.3$).

3.2. Flow Regimes of MSM. We assume that the HW is divided into three PS with the same interval, and each PS has the same length, since production rate distribution has a distinct effect on PTB and flows regime. Here, we take $q_{wiD} = 0.1 : 0.3 : 0.6$ for example to analyze flow regimes of MSM, as shown in Figure 3. In detail, this section can be divided into four cases for further discussion according to the length of HW and PS.

Case 1 (long HW ($L = 1200$ m, $h = 100$ m, $\beta^2 = 0.1$))

Case 1-1. For short length of PS ($L_{wi} = 133$ m), type curves are shown in Figure 3(a). The wellbore storage flow is the first regime, identified by a straight line with unit slope. The second period is transitional flow regime, controlled by a skin factor. After that, fluids flow into HW radially from the formation, which is acknowledged as the early radial flow regime. With pressure further spreading, spherical flow occurs when the predominant flow pattern is towards a point, which is recognized as −0.5 slope on the pressure derivative curve. Since the length of HW is long and the length of PS is quite short, intermediate radial flow appears around each PS. When the effect of the bottom water reaches the HW, the reservoir receives energy supplement and pressure tends to be stable gradually, known as the steady flow regime.

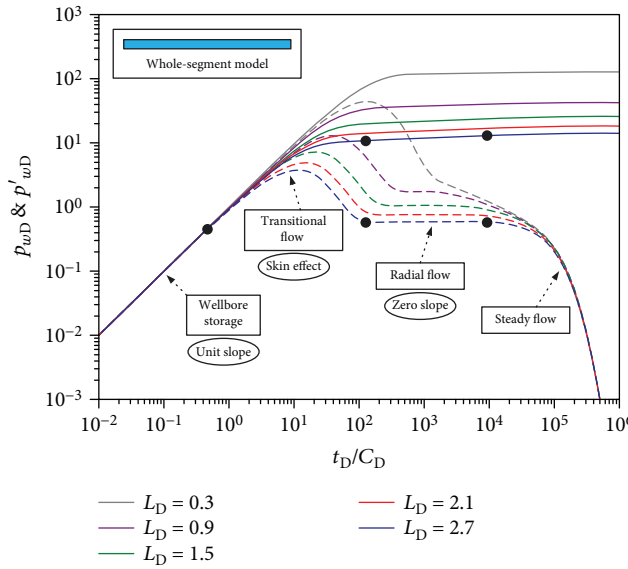

Figure 2: Type curves of WSM of HW subject to bottom water drive.

Case 1-2. For the long length of PS ($L_{wi} = 360$ m), type curves are shown in Figure 3(b). Flow regimes still include wellbore storage flow, transitional flow regime, and early radial flow. After that, fluid flows from outer zones and the pressure derivative curve shows a straight line with 0.36 slope. Tiab [60] derived the relationship between $(P'_D \times t_D)$ vs. (t_D) and named this flow regime as elliptical flow. Finally, the effect of the bottom water reaches the HW, which leads to a steady flow regime.

Case 2 (short HW ($L = 300$ m, $h = 100$ m, $\beta^2 = 0.1$))

Case 2-1. For short length of PS ($L_{wi} = 20$ m), type curves are shown in Figure 4(a). Different from Case 1, early radial flow disappears since the length of HW is short in Case 2. The pressure response for the short length of PS (L_{wi}) yields four flow regimes: wellbore storage flow, transitional flow, elliptical flow, and steady flow.

Case 2-2. For the long length of PS ($L_{wi} = 90$), spherical flow with −0.5 slope disappears compared with that when the length of HW is long (e.g., $L = 1200$ m). As a result, the flow regimes include wellbore storage flow, transitional flow, linear flow, and steady flow regime. Furthermore, the duration of elliptical flow lasts longer compared with Case 2.1, as shown in Figure 4(b).

4. Sensitivity Analysis

The total production rate should be kept the same for different cases. The effect of crucial parameters (e.g., production rate distribution, the length of HW, the length of PS, the number of PS, PS spacing, skin factor, and anisotropy degree) is shown in Figures 5–12.

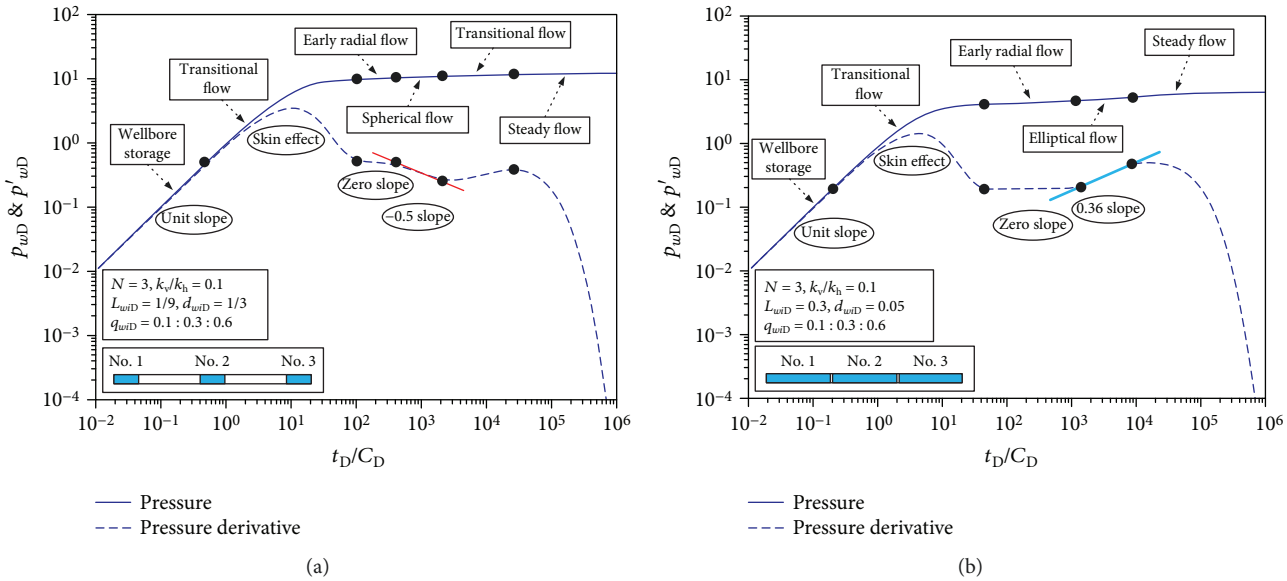

Figure 3: Type curves of MSM when the length of HW is long: (a) with short length of PS and (b) with long length of PS.

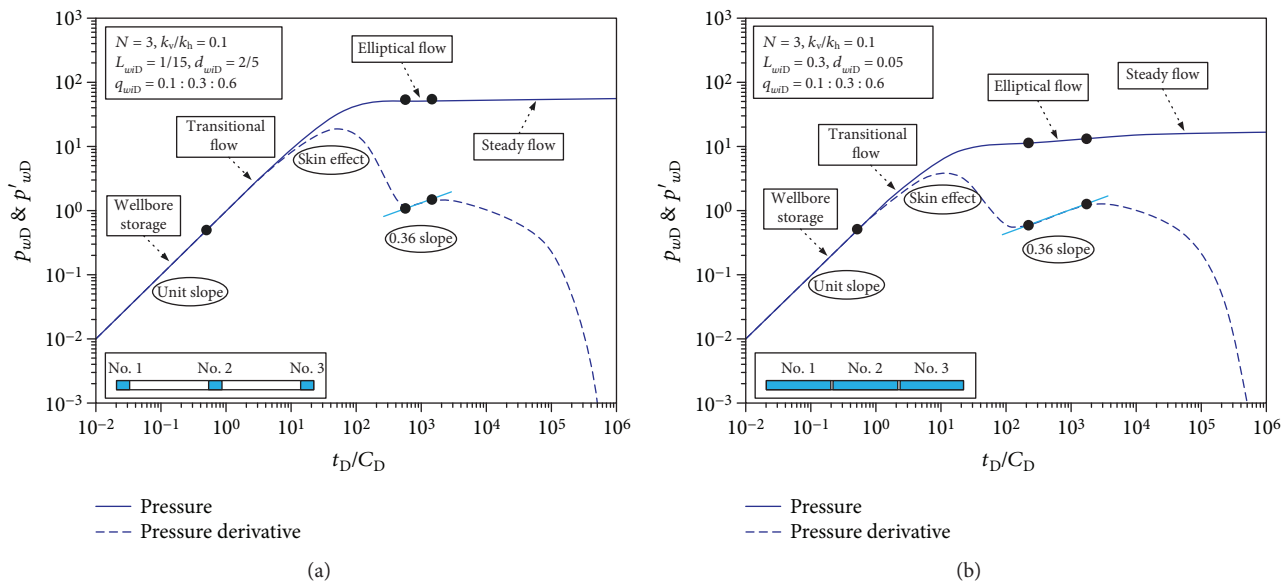

Figure 4: Type curves of MSM when the length of HW is short: (a) with short length of PS and (b) with long length of PS.

4.1. Production Rate Distribution

4.1.1. Effect of Production Rate of Constant PS. An HW with a length of 1200 m is divided into four PS with equal length of 300 m. The dimensionless production rate of each PS is defined as q_{wiD}. To discuss the effect of the production rate of a specific PS (i.e., q_{w1D}, q_{w2D}, q_{w3D}, and q_{w4D}) on PTB, the production rate of other PS remain constant and equal to each other (i.e., $q_{w2D} = q_{w3D} = q_{w4D}$, $q_{w1D} = q_{w3D} = q_{w4D}$, $q_{w1D} = q_{w2D} = q_{w4D}$, and $q_{w1D} = q_{w2D} = q_{w3D}$). Figures 5(a)–5(d) show that q_{w1D} makes a visible influence on type curves. With the increase in q_{w1D}, type curves will move up overall. In detail, when the production rate distributes uniformly along the HW (e.g., $q_{w1D} = q_{w2D} = q_{w3D} = q_{w4D} = 3/12$), the early radial flow starts at $t_D/C_D = 110$ and ends at $t_D/C_D = 12{,}000$, which shows the longest period of early radial flow compared with other conditions of production rate distribution. The value of the pressure derivative during this flow period equals to 0.9. Then, with the increase in q_{w1D} (e.g., $q_{w1D} = 4/12$, $q_{w1D} = 6/12$, $q_{w1D} = 9/12$, and $q_{w1D} = 12/12$), dimensionless pressure and its derivative curves will move up, and vice versa (e.g., $q_{w1D} = 2/12$, $q_{w1D} = 1/12$, and $q_{w1D} = 0/12$). Furthermore, when only one PS produces, as the distance of producing PS to the heel of HW becomes nearer (e.g., $q_{wiD} = 0 : 0 : 0 : 1$, $q_{wiD} = 0 : 0 : 1 : 0$, $q_{wiD} = 0 : 1 : 0 : 0$, and $q_{wiD} = 1 : 0 : 0 : 0$),

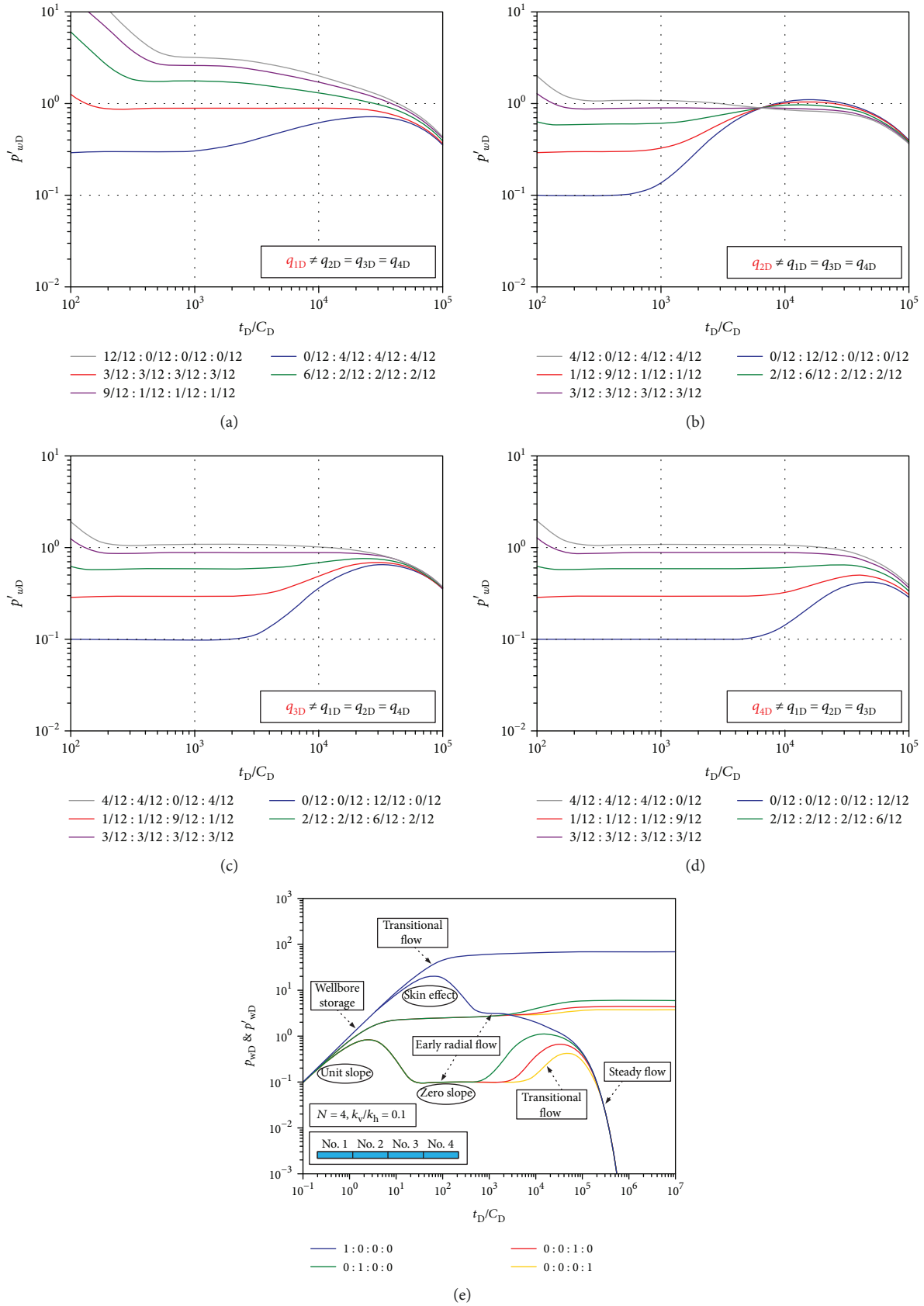

Figure 5: Effect of production rate of specific PS on PTB: (a) $q_{w1D} \neq q_{w2D} = q_{w3D} = q_{w4D}$, (b) $q_{w2D} \neq q_{w1D} = q_{w3D} = q_{w4D}$, (c) $q_{w3D} \neq q_{w1D} = q_{w2D} = q_{w4D}$, (d) $q_{w4D} \neq q_{w1D} = q_{w2D} = q_{w3D}$, and (e) comparison between the above four cases.

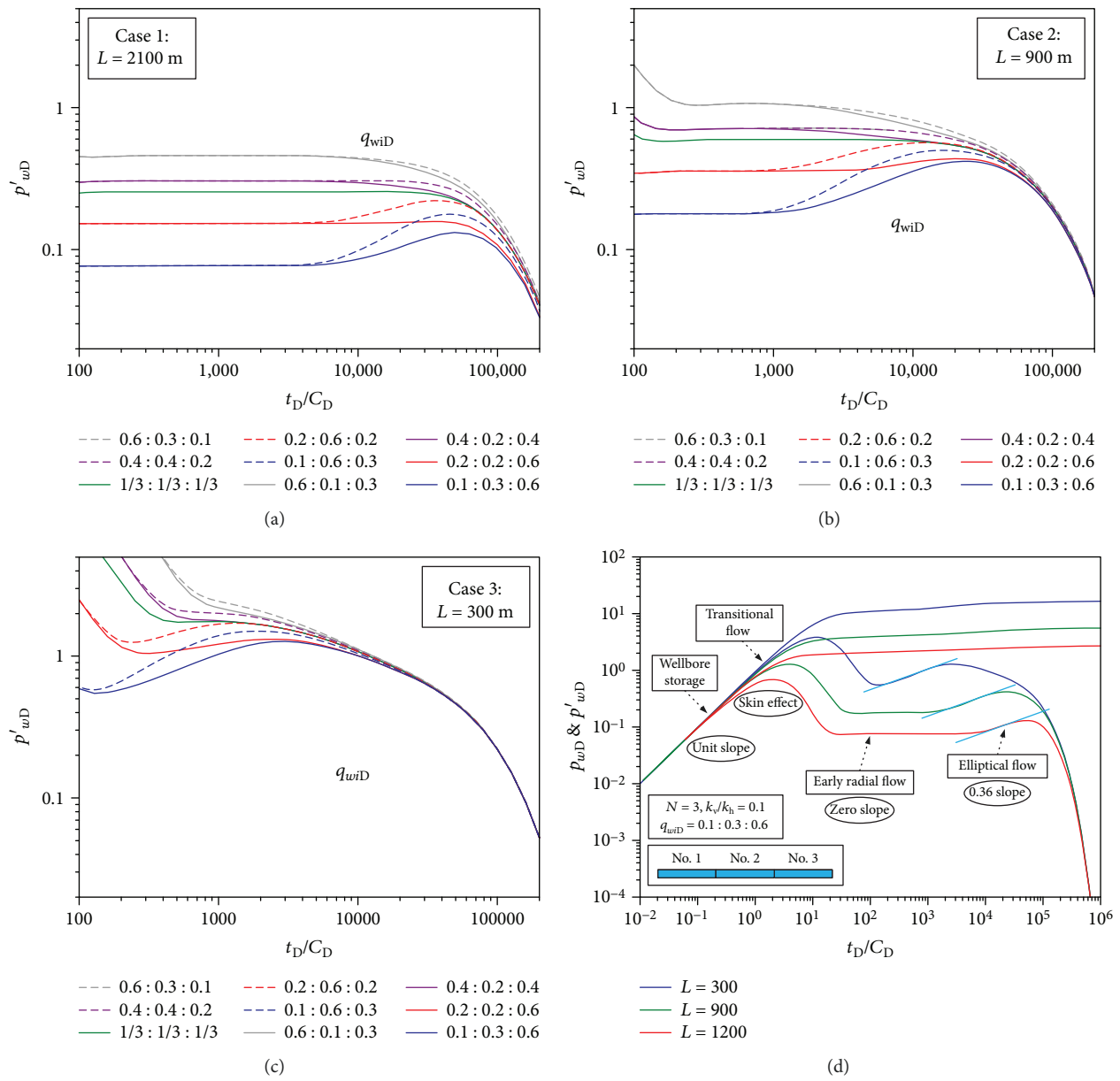

Figure 6: Effect of production rate distribution on PTB under different lengths of HW: (a) $L = 2100$ m, (b) $L = 900$ m, (c) $L = 300$ m, and (d) comparison between above three cases.

transitional flow lasts longer while early radial flow becomes shorter, shown in Figure 5(e). When the well is water-out, the production at water-influx locations will be much higher than that at other locations. Therefore, the water-influx locations cannot be diagnosed if the effect of nonuniform production distribution on pressure response was neglected.

4.1.2. Effect of Production Rate Distribution under Different Lengths of HW. Since the length of HW affects flow regimes of MSHW subject to bottom-water drive distinctly, three cases are selected according to the length of HW to eliminate the possibility that the length of HW may disturb the effect of production rate distribution on PTB.

The HW with length of L (i.e., 2100 m, 900 m, and 300 m) consists of three PS. The dimensionless length of each PS equals to 1/3, and the total dimensionless length of PS equals to 1. We discuss the effect of different production rate distributions ($q_{wiD} = 0.1 : 0.3 : 0.6$, $q_{wiD} = 0.1 : 0.6 : 0.3$, $q_{wiD} = 0.2 : 0.2 : 0.6$, $q_{wiD} = 0.2 : 0.6 : 0.2$, $q_{wiD} = 1/3 : 1/3 : 1/3$, $q_{wiD} = 0.4 : 0.2 : 0.4$, $q_{wiD} = 0.4 : 0.4 : 0.2$, $q_{wiD} = 0.6 : 0.1 : 0.3$, and $q_{wiD} = 0.6 : 0.3 : 0.1$) on PTB under different lengths of HW, as shown in Figure 6.

In general, the following flow regimes (transitional flow, the early radial flow, and steady flow) are influenced by production rate distribution. It is clearly found that the magnitude of influence caused by production rate distribution on pressure drop are shown as (from high to low) q_{w1D} (dimensionless production rate of heel on HW), q_{w2D} (dimensionless production rate of middle section of HW), and q_{w3D} (dimensionless production rate of toe of HW).

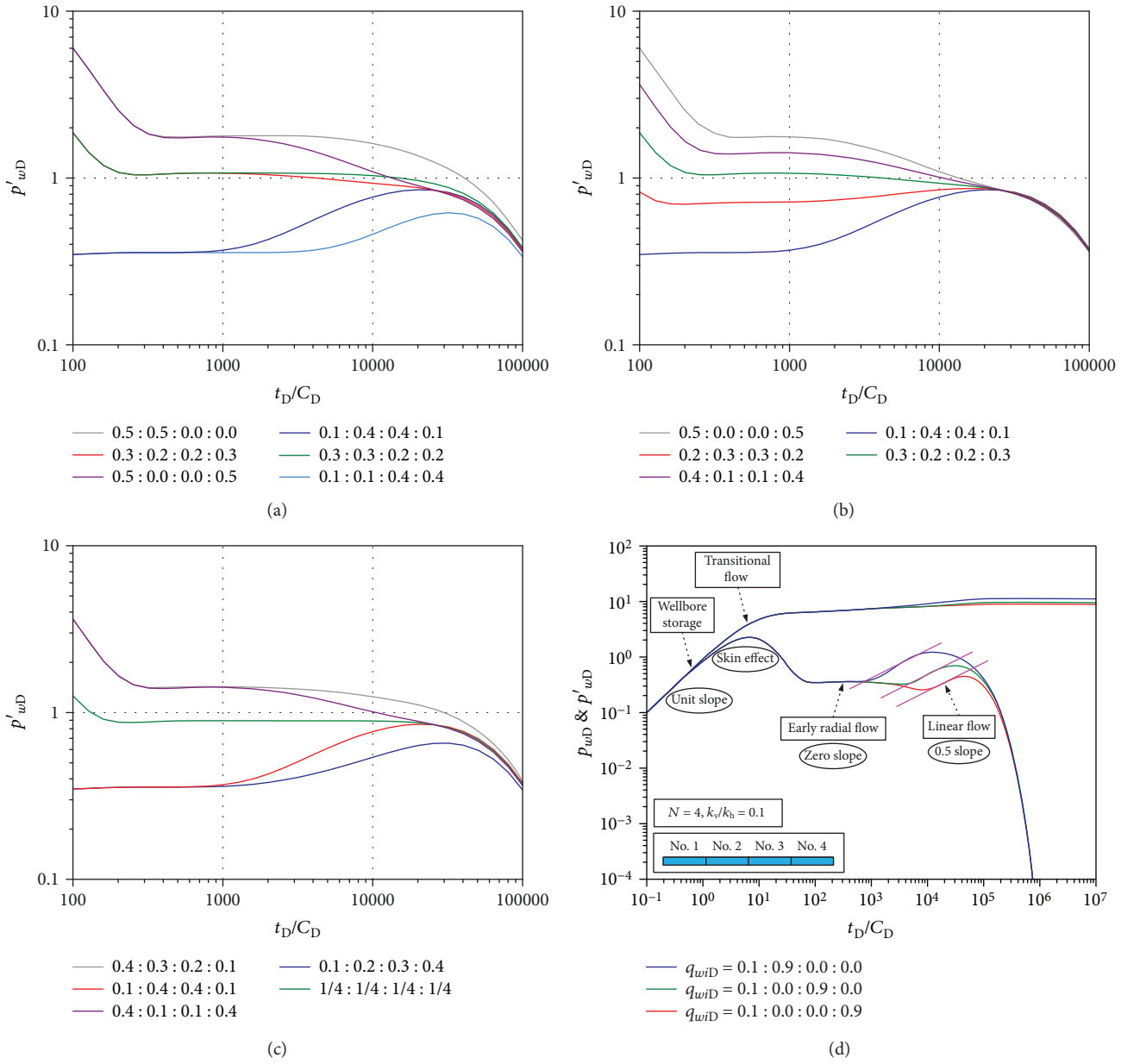

Figure 7: Effect of distribution pattern with four PS: (a) effect of q_{w2D}, (b) dumbbell-shaped/spindle-shaped distribution, (c) ladder shape distribution, and (d) with different location of the second PS.

Furthermore, these nine kinds of production rate distribution can be divided into four categories: $q_{w1D} = q_{w2D} = q_{w3D}$, $q_{w1D} = q_{w2D} \neq q_{w3D}$, $q_{w1D} \neq q_{w2D} = q_{w3D}$, and $q_{w1D} \neq q_{w2D} \neq q_{w3D}$. Specifically, when the production rate distributes uniformly (e.g., $q_{wiD} = 1/3 : 1/3 : 1/3$), the duration of early radial flow is the longest. When the production rate distributes nonuniformly, the value of q_{w2D} influences the characteristics of transitional flow between the early radial flow and steady flow (q_{w1D} is a constant). Type curves move up with the increase in q_{w2D} (e.g., $q_{wiD} = 0.1 : 0.3 : 0.6$, $q_{wiD} = 0.1 : 0.6 : 0.3$, and $q_{wiD} = 0.2 : 0.6 : 0.2$), and vice versa (e.g., $q_{wiD} = 0.4 : 0.2 : 0.4$, $q_{wiD} = 0.6 : 0.1 : 0.3$, and $q_{wiD} = 0.6 : 0.3 : 0.1$). Especially, if q_{w1D} equals to q_{w2D}, transitional flow will disappear (e.g., $q_{wiD} = 0.2 : 0.2 : 0.6$; $q_{wiD} = 0.4 : 0.4 : 0.2$). Type curves during the early steady flow regime will intersect with each other when q_{w1D} is equal to q_{w3D} (e.g., $q_{wiD} = 0.4 : 0.2 : 0.4$, $q_{wiD} = 1/3 : 1/3 : 1/3$, and $q_{wiD} = 0.2 : 0.6 : 0.2$).

In addition, by comparing the results from Figures 6(a)–6(c), results show that the length of HW only affects the positions of type curves and duration of each flow regime, and it does not influence the typical characteristics of type curves, as shown in Figure 6(d). In these three cases, flow regimes include wellbore storage flow, transitional flow, early radial flow, and elliptical flow which appear before the steady flow regime.

4.1.3. Effect of Different Production Distributions of PS. In this part, an HW with the length of 1200 m is divided into four

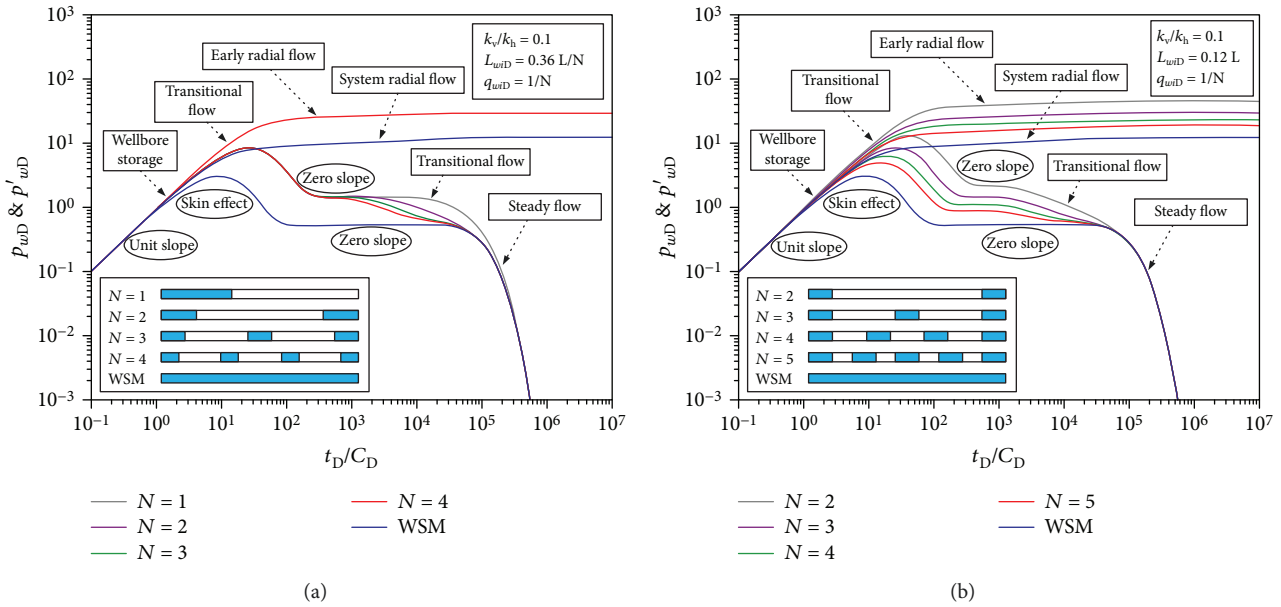

Figure 8: Effect of number of PS on PTB when the total length of PS is (a) constant and (b) variable.

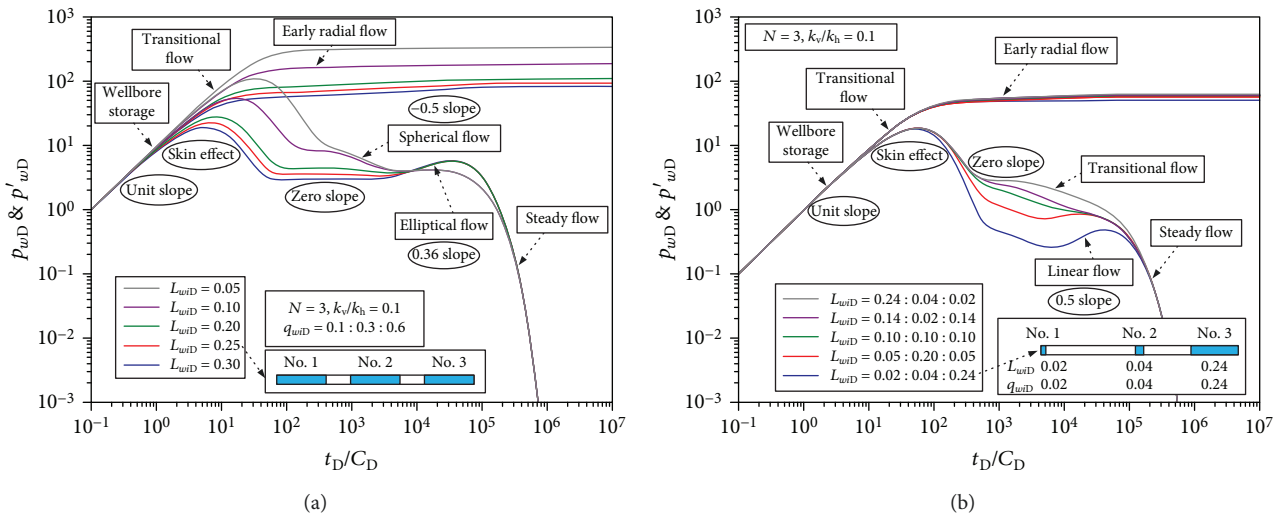

Figure 9: Effect of length of PS on PTB: (a) UDLPS and (b) NDLPS.

PS. Figure 7 indicates that pressure and its derivative curves are upper with a higher production rate of the first PS (e.g., q_{w1D} increases from 0.1 to 0.5) during flow regimes including transitional flow, the early radial flow, and steady flow regimes. As pressure further spreads, type curves will bifurcate when q_{w2D} is unequal during the early radial flow regime (e.g., $q_{w1D} = 0.1$, $q_{w2D} = 0.1$, and $q_{w2D} = 0.4$; $q_{w1D} = 0.3$, $q_{w2D} = 0.2$, and $q_{w2D} = 0.3$; and $q_{w1D} = 0.5$, $q_{w2D} = 0.0$, and $q_{w2D} = 0.5$), based on Figure 7(a). Additionally, type curves are lower when q_{w2D} is smaller than q_{w1D} (e.g., $q_{w2D} = 0.0 < 0.5 = q_{w1D}$; $q_{w2D} = 0.2 < 0.3 = q_{w1D}$), and type curves are higher when q_{w2D} is bigger than q_{w1D} (e.g., $q_{w2D} = 0.4 > 0.1 = q_{w1D}$) since a higher production rate leads to a bigger pressure drop. Apparently, Figures 7(b) and 7(c) demonstrate that the early radial flow is distinct when the production rate distribution pattern behaves as dumbbell-shaped (e.g., $q_{wiD} = 0.5 : 0.0 : 0.0 : 0.5$; $q_{wiD} = 0.4 : 0.1 : 0.1 : 0.4$) and spindle-shaped (e.g., $q_{wiD} = 0.1 : 0.4 : 0.4 : 0.1$). However, due to the strong interference of bottom-water, the value of the horizontal line does not equal to 0.5 during the early radial flow regime. Besides, according to Figure 7(c), pressure derivative curves will intersect at the early steady flow regime when the production rate of the first and last PS are equal (e.g., $q_{wiD} = 0.1 : 0.4 : 0.4 : 0.1$, $q_{wiD} = 0.4 : 0.1 : 0.1 : 0.4$, and $q_{wiD} = 1/4 : 1/4 : 1/4 : 1/4$) compared with the ladder shape (e.g., $q_{wiD} = 0.1 : 0.2 : 0.3 : 0.4$; $q_{wiD} = 0.4 : 0.3 : 0.2 : 0.1$). Finally, we discussed the situation when only two segments are producing. Figure 7(d) shows that the early radial flow lasts longer while the linear flow with 0.5 slope appears

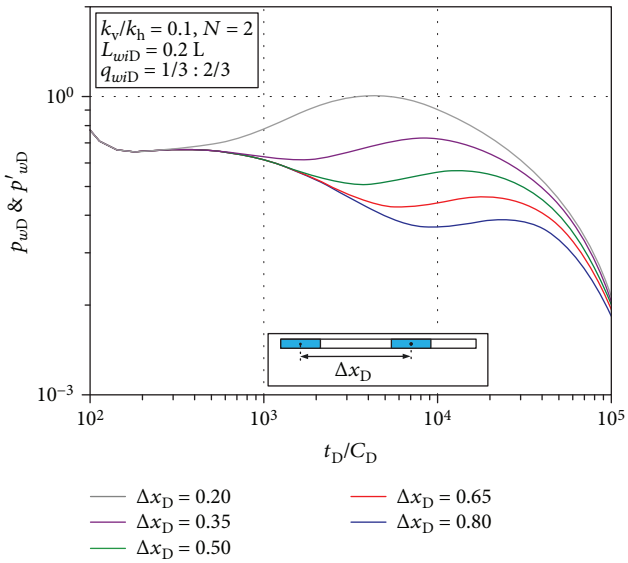

Figure 10: Effect of PS spacing on PTB.

later as the second PS is far from the heel of HW (e.g., $q_{wiD} = 0.1 : 0.9 : 0.0 : 0.0$, $q_{wiD} = 0.1 : 0.0 : 0.9 : 0.0$, and $q_{wiD} = 0.1 : 0.0 : 0.0 : 0.9$).

4.2. Number of PS. In this section, the number of PS (N) ranges from 2 to 5. For further discussion, this section is divided into two parts.

4.2.1. Constant Total Length of PS. In this part, the total length of PS equals to 0.36 L/N for MSM, while it is equal to L for WSM. Parameters (e.g., length, production rate, and skin factor of each PS) distribute uniformly along HW, and the total production rate remains constant for different cases. As shown in Figure 8(a), obvious differences exist among type curves of WSM and MSM except for the wellbore storage flow and steady flow regime. The effect of the number of PS on type curves for MSM can be observed during early radial flow and transitional flow regime. As the number of PS increases, early radial flow lasts shorter and pressure drop decreases during the transitional flow regime. When the number of PS is big enough, the early radial flow will disappear and may be masked by transitional flow before the steady flow regime. Furthermore, the pressure derivative during the early radial flow regime remains constant for a different number of PS (e.g., $N = 1, 2, 3, 4$).

4.2.2. Variable Total Length of PS (Constant Length of Each PS). In this part, the length of each PS equals to 0.12 L for MSM so that the total length of PS is variable for MSM. The length of PS for WSM still equals to L. The total skin factor and total production rates are kept constant for different cases. As shown in Figure 8(b), it is obvious that there exist obvious differences during early radial flow and transitional flow. Particularly, unlike the results from case one (total length of PS is constant), the duration of early radial flow does not change as the number of PS increases, while early radial flow and transitional flow regime appear earlier with the increase in the number of PS. Furthermore, since the total length of PS is variable, WSM is a specific situation of MSM when the number of PS is close to eight. In this case, transition flow will be covered by the steady flow.

4.3. Length of PS. The length of PS distribution can be classified into two categories: uniformly and nonuniformly. First, we discuss the effect of uniformly distributed length of PS (UDLPS) on type curves in this section. An HW is divided into three PS with equal length (e.g., $L_{wiD} = 0.05$, 0.10, 0.20, 0.25, 0.30), as shown in Figure 9(a). It is clearly observed that only wellbore storage flow and steady flow regimes are not influenced by the length of PS. Particularly, when L_{wiD} equals to 0.05, spherical flow appears since the predominant flow pattern in the reservoir is toward a point. Then, as L_{wiD} increases gradually, spherical flow disappears while elliptical flow with 0.36 slope appears following early radial flow.

For further discussion, we investigate the effect of nonuniformly distributed length of PS (NDLPS) (e.g., $L_{wiD} = 0.24 : 0.04 : 0.02$, $0.14 : 0.02 : 0.14$, $0.10 : 0.10 : 0.10$, $0.05 : 0.20 : 0.05$, and $0.02 : 0.04 : 0.24$) on pressure drop. As shown in Figure 9(b), obvious distinctions can be observed during flow regimes including early radial flow and transitional flow regimes which are different from those of UDLPS. Furthermore, slopes of the transitional flow regime on pressure derivative curves are equal in this situation.

4.4. PS Spacing. A horizontal well with the length of 1000 m consists of two PS with the length of 200 m, one of which is located at the heel of HW. The dimensionless spacing between PS is defined as $\Delta x_D = (x_{w2} - x_{w1})/L$. Different dimensionless PS spacings ($\Delta x_D = 0.20$, 0.35, 0.50, 0.65, and 0.80) are taken into account for analyzing their effects on type curves, shown in Figure 10. In the following cases, other parameters (e.g., total production rate, the number of PS, and skin factor of each PS) are constant. There exist distinct differences during the early radial flow, transitional flow, and early steady flow regime when PS spacing varies from 0.20 to 0.80. As Δx_D increases, early radial flow lasts longer and pressure drop decreases during the transitional flow regime. In detail, when t_D/C_D equals to 10,000, the value of the pressure derivative changes from 0.35 to 0.9 as Δx_D changes from 0.20 to 0.80.

4.5. Skin Factor. A horizontal well with the length of 1000 m consists of four segments with the same length of PS ($L_{wiD} = 0.1$) and PS spacing (Δx_D). For further discussion, this section is divided into two cases.

4.5.1. Variable Total Skin Factor of PS (Equal Skin Factor of Each PS). In this situation, the skin factor of each PS is equal so that the total skin factor of PS is different for different situations. With the decrease in total skin factor ($S_i = 8 : 8 : 8 : 8$, $S_i = 4 : 4 : 4 : 4$, $S_i = 2 : 2 : 2 : 2$, $S_i = 1 : 1 : 1 : 1$, and $S_i = 0.5 : 0.5 : 0.5 : 0.5$), type curves during the transitional flow regime move down as shown in Figure 11(a).

4.5.2. Constant Total Skin Factor of PS. In this case, the total skin factor is constant. If the length and production rate of each PS are the same, the effect of the nonuniform

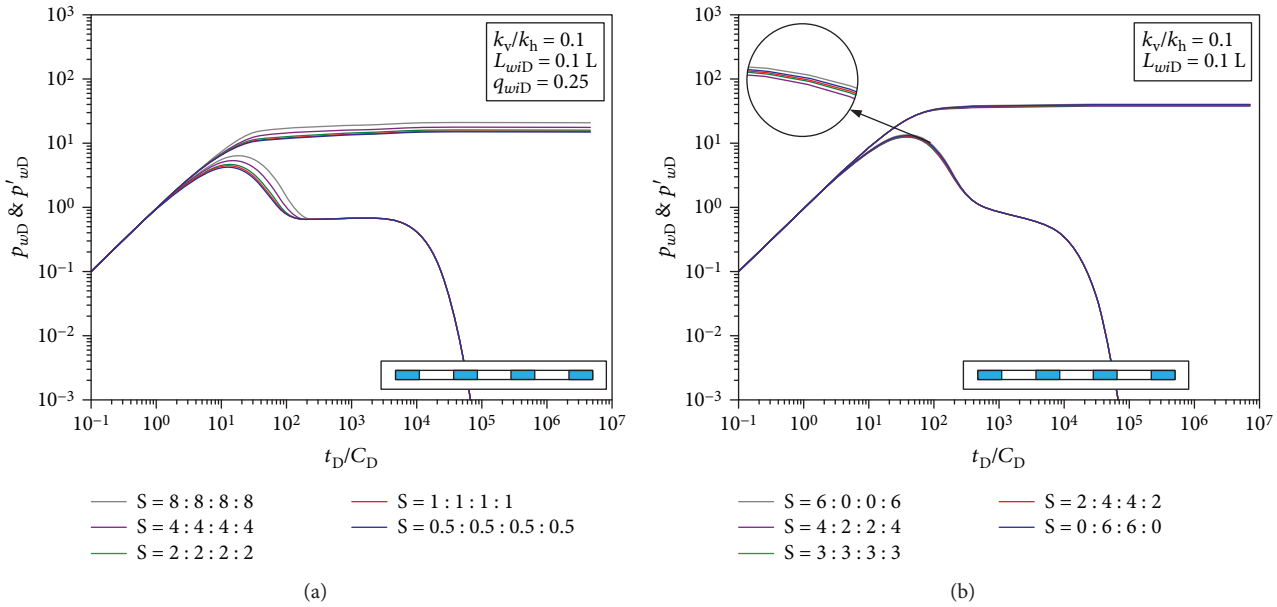

Figure 11: Effect of skin factor on PTB: (a) with variable total skin factor of PS and (b) with constant total skin factor of PS.

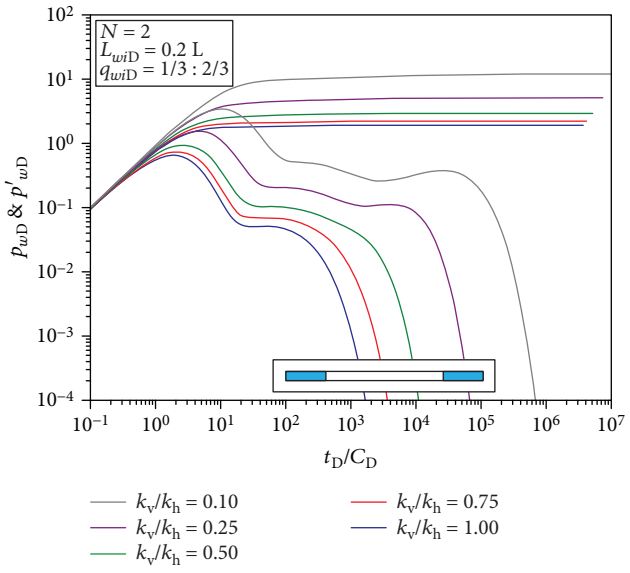

Figure 12: Effect of AD on PTB.

distribution of the skin factor on PTB is unapparent. This is because total pressure drop caused by skin effect depends on the length, production rate, and skin factor of each PS. When the length and production rate of each PS are different, slight distinctions can be observed on type curves, shown in Figure 11(b).

4.6. Anisotropy Degree. The HW with the length of 800 m consists of two segments located at the heel and toe of HW, respectively, as shown in Figure 12. Other parameters of each PS are kept the same (e.g., production rate, length, and skin factor). The anisotropy degree (AD) can be characterized using the ratio of vertical permeability to horizontal permeability ($AD = k_v/k_h$). When k_h remains at 1000 mD, AD can be changed by altering the value of k_v. The bottom water may rise faster when AD becomes bigger, and the well can receive energy supply earlier so that the late steady flow regime will occur early. Additionally, the early-radial flow regime will disappear as the AD increases, and the typical characteristic of the MSHW model will be covered when k_v is higher than 500 mD, which is adverse for diagnosis. The strong influence of the bottom water will increase the multiplicity of well-testing interpretation, so that this model is available when k_v is lower than 500 mD.

5. Limitations and Future Work

The strong influence caused by bottom water will increase the multiplicity of well-testing interpretation, so that this model is available when k_v is lower than 500 mD. Since only single-phase fluid is incorporated in the model, the proposed model is mainly used to solve the interpretation of those wells whose water cut are close to 100%.

Therefore, the multiphase model of MSHW may be established to better distinguish the water and oil production profile based on field test data. Furthermore, novel methods need to be developed to reduce the nonuniqueness of pressure interpretation with strong bottom water drive.

6. Conclusions

A novel approach was presented for determining nonuniform production distribution as well as detecting the location of water entry. First, HW is divided into multiple segments with arbitrary parameters (e.g., production, length, location, and skin factor). Then, new pressure transient solutions for HW are derived in the anisotropic reservoir with bottom-water drive. Clear distinctions can be observed between type

curves of MSM and WSM. As a result, neglecting nonuniform production distribution along the wellbore could lead to erroneous results for detecting the location of water entry. The early radial flow regime of MSM appears later than WSM. Spherical flow and elliptical flow regimes appear on type curves of MSM which do not exist on that of WSM.

Sensitivity analysis shows that anisotropy degree and production rate distribution play important roles in pressure response, followed by length, number, spacing, and skin factor of PS. When the total skin factor remains constant, the effect of the nonuniform distribution of skin factor on pressure response can be ignored. Additionally, the late stable flow appears earlier with increasing vertical permeability, which covers up the early radial flow and is bad for parameter estimation. Besides, water controlling for water-out segments and stimulation treatments for nonproducing segments can be carried out to improve oil recovery based on interpretation results.

Nomenclature

C: Wellbore storage coefficient, atm^{-1}
C_D: Dimensionless wellbore storage coefficient
C_t: Total compressibility, atm^{-1}
h: Formation thickness, cm
h^*: Formation thickness considering permeability anisotropy, cm
$h_D{}^*$: Dimensionless formation thickness considering permeability anisotropy
k_h: Horizontal permeability, D
k_v: Vertical permeability, D
L: Total length of HW, cm
L_D: Dimensionless length of HW
L_{Di}: Ratio of the i^{th} segment length to formation thickness considering anisotropy
L_{wi}: Length of the i^{th} segment, cm
L_{wiD}: Ratio of the i^{th} segment length to total length of HW
N: Number of PS, dimensionless
p: Pressure, atm
p_i: Initial reservoir pressure, atm
p_D: Dimensionless pressure drop
p_{SD}: Dimensionless transient pressure solution considering the effect of skin factor
p_{wD}: Dimensionless transient pressure solution considering wellbore-storage effect
q: Total production rate, cm^3/s
q_{wi}: Production rate of the i^{th} segment, cm^3/s
q_{wiD}: Dimensionless production rate of the i^{th} segment, cm^3/s
r_w: Wellbore radius, cm
r_{wD}: Dimensionless wellbore radius
S: Skin factor
S_{wi}: Skin factor of the i^{th} segment
t: Time, s
t_D: Dimensionless time
u: Laplace transform variable
x, y, z: Cartesian coordinates
x_D, y_D, z_D: Dimensionless Cartesian coordinate
x_{wi}, y_{wi}, z_{wi}: Coordinates of the center of the i^{th} segment
$x_{wiD}, y_{wiD}, z_{wiD}$: Dimensionless coordinates of the center of the i^{th} segment
z^*: z-Coordinate considering permeability anisotropy, cm
ϕ: Porosity, fraction
η_h: Diffusivity in horizontal direction, cm^3/s
η_v: Diffusivity in vertical direction, cm^3/s
μ: Fluid viscosity, cP
β: Anisotropy coefficient
τ: Time variable
Δp: Pressure drop caused by the i^{th} segment
$\bar{p}_{wD}$: Dimensionless pressure solution in Laplace space.

Conflicts of Interest

The authors declare that they have no conflicts of interest.

Acknowledgments

The authors would like to thank the National Natural Science Foundation of China (No. U1762101) and National Science and Technology Major Projects (No. 2017ZX05009-003).

References

[1] F. M. Giger, L. H. Reiss, and A. P. Jourdan, "The reservoir engineering aspects of horizontal drilling," in *Proceedings of the SPE Annual Technical Conference and Exhibition, Society of Petroleum Engineers*, Houston, TX, USA, September 1984.

[2] E. Ozkan, *Performance of Horizontal Wells, [Ph.D. Thesis]*, University of Tulsa, Tulsa, OK, USA, 1988.

[3] J. Hu, C. Zhang, Z. Rui, Y. Yu, and Z. Chen, "Fractured horizontal well productivity prediction in tight oil reservoirs," *Journal of Petroleum Science and Engineering*, vol. 151, pp. 159–168, 2017.

[4] E. Ozkan and R. Raghavan, "Performance of horizontal wells subject to bottomwater drive," *SPE Reservoir Engineering*, vol. 5, no. 3, pp. 375–383, 1990.

[5] F. J. Kuchuk, P. A. Goode, D. J. Wilkinson, and R. K. M. Thambynayagam, "Pressure-transient behavior of horizontal wells with and without gas cap or aquifer," *SPE Formation Evaluation*, vol. 6, no. 1, pp. 86–94, 1991.

[6] T. Guo, Y. Li, Y. Ding, Z. Qu, N. Gai, and Z. Rui, "Evaluation of acid fracturing treatments in shale formation," *Energy & Fuels*, vol. 31, no. 10, pp. 10479–10489, 2017.

[7] S. J. H. Al Rbeawi and D. Tiab, "Effect of the number and length of zonal isolations on pressure behavior of horizontal wells," in *Proceedings of the SPE Production and Operations Symposium, Society of Petroleum Engineers*, Oklahoma City, OK, USA, March 2011.

[8] H. Tang, Z. Chai, B. Yan, and J. Killough, "Application of multi-segment well modeling to simulate well interference," in *Proceedings of the Unconventional Resources Technology Conference*, Austin, TX, USA, 2017.

[9] G. Cui, S. Ren, Z. Rui, J. Ezekiel, L. Zhang, and H. Wang, "The influence of complicated fluid-rock interactions on the geothermal exploitation in the CO_2 plume geothermal system," *Applied Energy*, vol. 227, pp. 49–63, 2018.

[10] M. A. Bawazir, H. N. Haji Ahmad, M. Zeybek, and S. Malik, "Pinpointing water entries in dead horizontal wells," in *Proceedings of the International Petroleum Technology Conference, American Association of Petroleum Geologists*, Bangkok, Thailand, November 2011.

[11] Y. He, S. Cheng, L. Li et al., "Waterflood direction and front characterization with four-step work flow: a case study in Changqing oil field, China," *SPE Reservoir Evaluation & Engineering*, vol. 20, no. 3, pp. 708–725, 2017.

[12] T. Yildiz, "The impact of nonuniform formation damage on horizontal well performance," in *Proceedings of the SPE International Symposium and Exhibition on Formation Damage Control, Society of Petroleum Engineers*, Lafayette, LA, USA, February 2006.

[13] Z. Rui, J. Lu, Z. Zhang et al., "A quantitative oil and gas reservoir evaluation system for development," *Journal of Natural Gas Science and Engineering*, vol. 42, pp. 31–39, 2017.

[14] Z. Rui, C. Li, F. Peng et al., "Development of industry performance metrics for offshore oil and gas project," *Journal of Natural Gas Science and Engineering*, vol. 39, pp. 44–53, 2017.

[15] Y. He, S. Cheng, L. Li et al., "Waterflood direction and front characterization with multiple methods: a case study in Changqing oilfield, China," in *Proceedings of the SPE Oil & Gas India Conference and Exhibition, Society of Petroleum Engineers*, Mumbai, India, November 2015.

[16] Z. Rui, F. Peng, K. Ling, H. Chang, G. Chen, and X. Zhou, "Investigation into the performance of oil and gas projects," *Journal of Petroleum Science and Engineering*, vol. 38, pp. 12–20, 2017.

[17] J. Rounce, C. Lenn, and G. Catala, "Pinpointing fluid entries in producing wells," in *Proceedings of the Middle East Oil Show and Conference, Society of Petroleum Engineers*, Bahrain, February 1999.

[18] A. M. Al-Behair, M. Zeybek, S. Malik, S. Lyngra, and A. Al-Hajari, "Real time diagnostics of gas entries and remedial shut-off in barefoot horizontal wells," in *Proceedings of the International Petroleum Technology Conference, American Association of Petroleum Geologists*, Dubai, UAE, December 2007.

[19] A. S. Al-Muthana, S. M. Ma, M. Zeybek, and S. Malik, "Comprehensive reservoir characterization with multiphase production logging," in *Proceedings of the SPE Saudia Arabia Section Technical Symposium, Society of Petroleum Engineers*, Al-Khobar, Saudi Arabia, May 2008.

[20] M. Aibazarov, A. Khassanova, P. Hutson et al., "The application of multi-sensor production logging and spectral noise logging tools in optimising water shut-off in a carbonate environment," in *Proceedings of the SPE Annual Caspian Technical Conference & Exhibition, Society of Petroleum Engineers*, Astana, Kazakhstan, November 2016.

[21] Y. Zheng, Y. Li, H. Zheng et al., "First horizontal-well production logging and water control success in a tough completion offshore well: a case study from China," in *Proceedings of the SPE Annual Technical Conference and Exhibition, Society of Petroleum Engineers*, San Antonio, TX, USA, October 2012.

[22] T. AlSharif, B. AlMalki, M. Bawazir, M. Zeybek, and Z. Zaouali, "Inflow profiling in challenging complex deep gas environment," in *Proceedings of the SPE Middle East Oil and Gas Show and Conference, Society of Petroleum Engineers*, Manama, Bahrain, March 2013.

[23] S. Sanjaya, L. Quintero, M. S. Lyer et al., "Water source and flow direction detection in a heterogeneous fracture carbonate reservoir: challenge and solutions_a case study in Indonesia," in *Proceedings of the Offshore Technology Conference-Asia, Offshore Technology Conference*, Kuala Lumpur, Malaysia, March 2014.

[24] R. Bhagavatula, M. F. Al-Ajmi, M. O. Awad et al., "An integrated downhole production logging suite for locating water sources in oil production wells," in *Proceedings of the SPE Oil & Gas India Conference and Exhibition, Society of Petroleum Engineers*, Mumbai, India, November 2015.

[25] Y. He, S. Cheng, J. Qin et al., "Successful application of well testing and electrical resistance tomography to determine production contribution of individual fracture and water-breakthrough locations of multifractured horizontal well in Changqing oil field, China," in *Proceedings of the SPE Annual Technical Conference and Exhibition, Society of Petroleum Engineers*, San Antonio, TX, USA, 2017.

[26] J. Qin, S. Cheng, Y. He et al., "Estimation of non-uniform production rate distribution of multi-fractured horizontal well through pressure transient analysis: model and case study," in *Proceedings of the SPE Annual Technical Conference and Exhibition, Society of Petroleum Engineers*, San Antonio, TX, USA, October 2017.

[27] D. W. Marquardt, "An algorithm for least-squares estimation of nonlinear parameters," *Journal of the Society for Industrial and Applied Mathematics*, vol. 11, no. 2, pp. 431–441, 1963.

[28] G. Brown, D. Storer, K. McAllister, M. Al-Asimi, and K. Raghavan, "Monitoring horizontal producers and injectors during cleanup and production using fiber-optic-distributed temperature measurements," in *Proceedings of the SPE Annual Technical Conference and Exhibition, Society of Petroleum Engineers*, Denver, CO, USA, October 2003.

[29] V. I. Fryer, S. Dong, Y. Otsubo, G. Brown, and P. Guilfoyle, "Monitoring of real-time temperature profiles across multizone reservoirs during production and shut in periods using permanent fiber-optic distributed temperature systems," in *Proceedings of the SPE Asia Pacific Oil and Gas Conference and Exhibition, Society of Petroleum Engineers*, Jakarta, Indonesia, April 2005.

[30] G. Brown, "Monitoring multilayered reservoir pressures and GOR changes over time using permanently installed distributed temperature measurements," in *Proceedings of the SPE Annual Technical Conference and Exhibition, Society of Petroleum Engineers*, San Antonio, TX, USA, September 2006.

[31] T. D. Bui, O. A. Vicencio, S. Sinha, R. Vicencio, and Y. Jalali, "In-situ diagnosis of inflow behavior in horizontal wells," in *Proceedings of the SPE International Improved Oil Recovery Conference in Asia Pacific, Society of Petroleum Engineers*, Kuala Lumpur, Malaysia, October 2003.

[32] G. Aggrey, D. R. Davies, and L. T. Skarsholt, "A novel approach of detecting water influx time in multi-zone and multilateral completions using real-time downhole pressure data," in *Proceedings of the SPE Middle East Oil and Gas Show and Conference, Society of Petroleum Engineers*, Manama, Bahrain, March 2007.

[33] K. Yoshioka, D. Zhu, A. D. Hill, P. Dawkrajai, and L. W. Lake, "A comprehensive model of temperature behavior in a horizontal well," in *Proceedings of the SPE Annual Technical Conference and Exhibition, Society of Petroleum Engineers*, Dallas, TX, USA, October 2005.

[34] K. Yoshioka, D. Zhu, A. D. Hill, P. Dawkrajai, and L. W. Lake, "Detection of water or gas entries in horizontal wells from temperature profiles," in *Proceedings of the SPE Europe/EAGE*

Annual Conference and Exhibition, Society of Petroleum Engineers, Vienna, Austria, June 2006.

[35] K. Yoshioka, D. Zhu, A. D. Hill, and L. W. Lake, "A new inversion method to interpret flow profiles from distributed temperature and pressure measurements in horizontal wells," *SPE Production & Operations*, vol. 24, no. 4, pp. 510–521, 2009.

[36] Z. Li and D. Zhu, "Predicting flow profile of horizontal wells by downhole pressure and DTS data for infinite waterdrive reservoir," in *Proceedings of the SPE Annual Technical Conference and Exhibition, Society of Petroleum Engineers*, New Orleans, LA, USA, October 2009.

[37] M. D. Clonts and H. J. Ramey, "Pressure transient analysis for wells with horizontal drainholes," in *Proceedings of the SPE California Regional Meeting, Society of Petroleum Engineers*, Oakland, CA, USA, April 1986.

[38] E. Ozkan, R. Raghavan, and S. D. Joshi, "Horizontal well pressure analysis," *SPE Formation Evaluation*, vol. 4, no. 4, pp. 567–575, 1989.

[39] M. D. Clonts and H. J. J. Ramey, "Pressure transient analysis for Wells with horizontal drainholes," in *Proceedings of the SPE California Regional Meeting*, Oakland, CA, USA, April 1986.

[40] F. Daviau, G. Mouronval, G. Bourdarot, and P. Curutchet, "Pressure analysis for horizontal wells," *SPE Formation Evaluation*, vol. 3, no. 4, pp. 716–724, 1988.

[41] T. Yildiz and E. Ozkan, "Transient pressure behaviour of selectively completed horizontal wells," in *Proceedings of the SPE Annual Technical Conference and Exhibition*, New Orleans, LA, USA, September 1994.

[42] X. Zhao, Z. Rui, X. Liao, and R. Zhang, "A simulation method for modified isochronal well testing to determine shale gas well productivity," *Journal of Natural Gas Science and Engineering*, vol. 27, no. 2, pp. 479–485, 2015.

[43] R. Aguilera and M. C. Ng, "Transient pressure analysis of horizontal wells in anisotropic naturally fractured reservoirs," *SPE Formation Evaluation*, vol. 6, no. 1, pp. 95–100, 1991.

[44] M. M. Kamal, I. M. Buhidma, S. A. Smith, and W. R. Jones, "Pressure-transient analysis for a well with multiple horizontal sections," in *Proceedings of the SPE Annual Technical Conference and Exhibition, Society of Petroleum Engineers*, Houston, TX, USA, October 1993.

[45] Y. He, S. Cheng, J. Qin et al., "A semianalytical approach to estimate the locations of malfunctioning horizontal wellbore through bottom-hole pressure and its application in Hudson oilfield," in *Proceedings of the SPE Middle East Oil & Gas Show and Conference, Society of Petroleum Engineers*, Manama, Bahrain, March 2017.

[46] J. Qin, S. Cheng, Y. He et al., "Rate decline analysis for horizontal wells with multiple sections," *Geofluids*, 2018, in press.

[47] S. J. H. Al Rbeawi and T. Djebbar, "Transient pressure analysis of a horizontal well with multiple inclined hydraulic fractures using type-curve matching," in *Proceedings of the SPE International Symposium and Exhibition on Formation Damage Control*, Lafayette, LA, USA, February 2012.

[48] J. Guo, B. Luo, C. Lu, J. Lai, and J. Ren, "Numerical investigation of hydraulic fracture propagation in a layered reservoir using the cohesive zone method," *Engineering Fracture Mechanics*, vol. 186, pp. 195–207, 2017.

[49] Y. He, S. Cheng, L. Hu et al., "A pressure transient analysis model of multi-fractured horizontal well in consideration of unequal production of each fracture," *Journal of China University of Petroleum (Edition of Natural Science)*, vol. 41, no. 4, pp. 116–123, 2017.

[50] J. Guo, J. Wang, Y. Liu, Z. Chen, and H. Zhu, "Analytical analysis of fracture conductivity for sparse distribution of proppant packs," *Journal of Geophysics and Engineering*, vol. 14, no. 3, pp. 599–610, 2017.

[51] J. Qin, Y. Liu, Y. Feng, Y. Ding, L. Liu, and Y. He, "New well pattern optimization methodology in mature low-permeability anisotropic reservoirs," *Journal of Geophysics and Engineering*, vol. 15, no. 1, pp. 93–105, 2018.

[52] Y. He, S. Cheng, S. Li et al., "A semianalytical methodology to diagnose the locations of underperforming hydraulic fractures through pressure-transient analysis in tight gas reservoir," *SPE Journal*, vol. 22, no. 3, pp. 924–939, 2017.

[53] W. Ren, S. Tian, G. Li, M. Sheng, and R. Yang, "Modeling of mixed-gas adsorption on shale using hPC-SAFT-MPTA," *Fuel*, vol. 210, pp. 535–544, 2017.

[54] A. C. Gringarten and H. J. Ramey, "The use of source and Green's functions in solving unsteady-flow problems in reservoirs," *Society of Petroleum Engineers Journal*, vol. 13, no. 5, pp. 285–296, 1973.

[55] X. Y. Kong, X. Z. Xu, and D. T. Lu, "Pressure transient analysis for horizontal well and multi-branched horizontal wells," in *Proceedings of the International Conference on Horizontal Well Technology, Society of Petroleum Engineers*, Calgary, Alberta, Canada, November 1996.

[56] A. B. Newman, "Heating and cooling rectangular and cylindrical solids," *Industrial & Engineering Chemistry*, vol. 28, no. 5, pp. 545–548, 1936.

[57] A. F. Van Everdingen, "The skin effect and its influence on the productive capacity of a well," *Journal of Petroleum Technology*, vol. 5, no. 6, pp. 171–176, 1953.

[58] A. F. Van Everdingen and W. Hurst, "The application of the Laplace transformation to flow problems in reservoirs," *Journal of Petroleum Technology*, vol. 1, no. 12, pp. 305–324, 1949.

[59] H. Stehfest, "Remark on algorithm 368: numerical inversion of Laplace transforms," *Communications of the ACM*, vol. 13, no. 10, p. 624, 1970.

[60] D. Tiab, "Analysis of pressure and pressure derivative without type-curve matching - III. Vertically fractured wells in closed systems," in *Proceedings of the SPE Western Regional Meeting, Society of Petroleum Engineers*, Anchorage, Alaska, May 1993.